Open Access Articles

The synthesis of cadmium sulfide nanoplatelets using a novel continuous flow sonochemical reactor

The Faculty of Oregon State University has made this article openly available.
Please share how this access benefits you. Your story matters.

Citation	Palanisamy, B., Paul, B., & Chang, C. H. (2015). The synthesis of cadmium sulfide nanoplatelets using a novel continuous flow sonochemical reactor. Ultrasonics Sonochemistry, 26, 452-460. doi:10.1016/j.ultsonch.2015.01.004
DOI	10.1016/j.ultsonch.2015.01.004
Publisher	Elsevier
Version	Accepted Manuscript
Terms of Use	http://cdss.library.oregonstate.edu/sa-termsofuse

Continuous sonochemical synthesis of cadmium sulfide nanoplatelets using an azeotropic solvent

Barath Palanisamy, Brian Paul and Chih-hung Chang

Oregon State University

Paper Highlights

- Developed a continuous flow chemical reactor for fast and controlled synthesis of CdS nanoplatelets
- Reduced processing time of CdS from 2 hours in batch ultrasound synthesis to less than a minute in continuous ultrasound synthesis
- Produced nanoplatelets of CdS averaging 21 nm with coefficient of variation of 25% and thickness below 10 nm
- Produced cubic phase CdS using continuous ultrasound synthesis approach

*Manuscript
Click here to view linked References

THE SYNTHESIS OF CADMIUM SULFIDE NANOPLATELETS USING A NOVEL CONTINUOUS FLOW SONOCHEMICAL REACTOR

Abstract

A continuous flow sonochemical reactor was developed capable of producing metastable cadmium sulfide (CdS) nanoplatelets with thicknesses at or below 10 nm. The continuous flow sonochemical reactor included the passive in-line micromixing of reagents prior to sonochemical reaction. Synthesis results were compared with those from reactors involving batch conventional heating and batch ultrasound-induced heating. The continuous sonochemical synthesis was found to result in high aspect ratio hexagonal platelets of CdS possessing cubic crystal structures with thicknesses well below 10 nm. The unique shape and crystal structure of the nanoplatelets are suggestive of high localized temperatures within the sonochemical process. The particle size uniformity and product throughput are much higher for the continuous sonochemical process in comparison to the batch sonochemical process and conventional synthesis processes.

1. Introduction

Cadmium sulfide (CdS) nanoparticles (NPs) exhibit quantum confinement effects as they approach the Bohr exciton radius below 10 nm. CdS is predominantly used as a buffer layer in different solar cells based on materials like CIGS [1], CIS [2] and in CdSe-Zn [3]. This critical layer improves photovoltaic device performance as well acts as a wide band transparent window to incoming sunlight. CdS is also used in a myriad of applications including lasers, waveguides, solar cells, photodetectors, photocatalysts and photodiodes [4]. To enable these applications, precise process control is necessary to minimize particle size distribution at small particle sizes.

It has been found that generally the particle size distribution for nanoparticles is narrower for sonocrystallization than for other comparable synthesis methods such as microfluidic-based routes. Table 1 shows a corresponding comparison of coefficient of variation (CV) based on data reported for these nanoparticle synthesis routes. Cadmium selenide data is compared since it is chemically similar to CdS in synthesis and structure.

Table 1. Nanoparticle size distributions reported in the literature

Material	Avg Size (nm)	SD (nm)	CV (%)	Synthesis Approach	Author
CdSe	8.0	0.6	8.0	Sonochem	Mastai et al [5]
CdSe	3.0	0.6	19.7	Sonochem	Mastai et al [5]
CdSe	4.0	0.7	17.0	Sonochem	Mastai et al [5]
CdSe	5.5	0.6	10.2	Sonochem	Mastai et al [5]
CdS	4.5	1.0	22.2	Microfluidic reactor	Peterson et al [6]
CdS	5.2	0.3	6.0	Microfluidic reactor	Wan et al [7]
CdS	5.5	0.9	16.4	Sonochem*	Wang et al [8]
CdS	11.5	6.5	56.3	Sonochem*	Wu et al [9]
CdS	8.5	3.5	40	Sonochem*	Gao et al [10]

*Data derived from results presented in the paper

In the sonochemical synthesis route, heating by cavitation and bubble implosion provides a potential route to high temperature reactions from a liquid phase. Sonochemistry has been used for the synthesis of nanoparticles of various semiconductor materials like CdS [11, 12] and PbS [13, 14] in batch modes. It has been demonstrated that a surfactant free approach using sonochemistry can be used to generate well dispersed CdS NPs [11]. However in batch mode, long residence times measured in hours can make process control more difficult due to the chemistry being exposed to the US energy multiple times. Further, batch US chemistries are difficult to scale-up. In continuous sonochemical synthesis, residence times can be reduced from several hours to less than a minute making it easier to control reaction conditions. Also, conventional solution processing does not yield high aspect ratio particles or high temperature phases. In general, very little research has been performed on continuous sonochemical synthesis [15, 16].

In this paper, a continuous flow sonochemical reactor is developed and used to continuously produce a metastable crystal structure in the form of high aspect ratio CdS platelets. The sub 10 nm thick platelets exhibit good particle size control without the use of surfactants. The method is compared with batch sonochemistry and conventional heating to delineate the advantages.

2. Development of a continuous flow sonochemical reactor

A flow cell reactor was developed to couple an ultrasonic (US) horn with the nanoparticle chemistry of interest. Ultrasound attenuates as a function of distance in front of the horn. Attenuation is an exponential function, strongly dependent on the attenuation coefficient (α) as given by [17]

$$\boldsymbol{I} = \boldsymbol{I}_0 \exp(-2\boldsymbol{\alpha d})$$

where I is intensity at distance d from the source, I_0 being initial intensity. The acoustic pressure amplitude as a function of distance from the horn has been modeled using the equation [18]

$$\boldsymbol{P(d)} = \boldsymbol{\rho c v}\left|2\sin\left(\frac{\boldsymbol{\pi}}{\boldsymbol{\lambda}}\left(\sqrt{\boldsymbol{d}^2+\boldsymbol{a}^2}-\boldsymbol{d}\right)\right)\right|$$

where P(d) is the acoustic pressure amplitude as a function of distance d, ρ is the density of the liquid, c is velocity of sound in the liquid, v is the velocity amplitude of the horn, λ is the wavelength of the sound and a is the radius of the horn tip.

A key factor in the design of the flow cell was to reduce the residence time of the flow chemistry within the reactor. Shorter residence times would lead to the potential for higher, more uniform power densities adjacent to the horn and less exposure to bulk temperatures. A horn with a maximum power inverter rating of 750 W (model VCX 750) and an interfacing flow cell (630-0495) were acquired from Sonics and Materials, Inc. To reduce fluid residence time within the flow cell, the internal volume of flow cell was modified through the use of an insert. Figure 1 shows a schematic of the internal volume of the reactor with and without the flow insert. The flow cell insert reduced the flow cell volume from 65 ml to 8 ml. The critical dimension in the insert was the clearance between the horn outer diameter and the inner diameter of the insert itself. This had to be sufficiently larger than the critical bubble size in order to prevent vapor lock restricting the outflow of processed reactants. The flow insert was made of UHMWPE due to its low density, high elasticity, high softening point and low cost.

The use of the insert was found to provide several benefits. First, Figure 2 shows the effect of the flow cell insert on the time needed for the bulk temperature to reach steady state in pure water. It can be clearly observed that it takes approximately one-third the amount of time to

reach 70°C for pure water. Second, the curve collected without the insert shows several points at which the temperature suddenly drops off. This is due to temperature accumulation adjacent to the horn leading to bubble accumulation and disruption of power transfer. This suggests that the use of the flow cell insert led to better temperature uniformity within the flow cell as originally intended. A schematic of the final continuous flow setup is shown in Figure 3.

Figure 1. Cross-section of continuous flow reactor a) without insert and b) with insert.

Figure 2. Effect of volume reduction on heating rate

Figure 3. Schematic of continuous sonochemical reactor setup

3. Experimental methods

Based on prior literature [10] , a cadmium chloride and thiourea reactant chemistry was chosen for sonochemical synthesis of cadmium sulfide nanoparticles. This chemistry involves processing at 85°C [19, 20]. The reaction mechanism involves forming a cadmium-thiourea complex – $Cd[SC(NH_2)_2](OH)_2$ which is aided by ammonia released from ammonium chloride-ammonium hydroxide buffer. This controls the release of Cd ions for precipitation into CdS and hence affects the kinetics of the reaction, aimed at controlling the particle size. Table 2 shows the conditions chosen for the reaction in batch and continuous modes. The chemistry was first evaluated in batch mode to check feasibility.

Table 2. Experimental conditions for sonochemical synthesis of CdS

Parameters	**Batch**	**Continuous**
Chemistry	$CdCl_2$ + $CS(NH_2)_2$ + NH_4Cl + NH_4OH	$CdCl_2$ + $CS(NH_2)_2$ + NH_4Cl + NH_4OH
Processing time	120 min	48 sec
Reynolds no	-	410
Ultrasound Power (Avg)	20 W	100 W

Since the boiling point of pure water is very close to the reaction temperature of 85°C, highly localized hot spots can result in vapor phase formation leading to flow disruption i.e. vapor lock. Hence an azeotropic mix consisting of water and ethylene glycol in a 1:1 volume was used, elevated the boiling point to 107°C [21]. The nanoparticles were quenched at the outlet, washed, dried and used for observation. A FEI TITAN Chemi-STEM (Portland, OR, USA) operating at 200 kV was used to image the nanoparticles. A Bruker-AXS D8 Discover X-ray diffraction unit (Madison, WI, USA) was used for phase analysis using XRD patterns. A SX-100 CAMECA electron microprobe analyzer (Gennevillier, France) was used to evaluate the composition of nanoparticles using wave dispersive spectroscopy (WDS). Unlike energy dispersive spectroscopy (EDS), WDS uses the wave nature of X-rays and Bragg's diffraction of the X-rays produced when an electron beam hits the surface of the sample. This has significant advantages over traditional EDS as it has better energy resolution, better detection of lighter elements and higher signal to noise ratio. A few milligrams of the nanoparticles were formed into a pellet on a glass substrate for this compositional analysis.

In sonochemical synthesis, low-frequency (20 – 100 kHz) sound waves are emitted from a horn and propagated through the solution in which the horn is submerged. The low-frequency ultrasound energy couples with the solvent producing fluid dynamic, thermal and chemical effects [22]. Ultrasonic energy is coupled with solvents via cavitation involving bubble nucleation, growth and collapse [23]. During the rarefaction half cycle the bubble grows and reaches a critical size before it implodes in a compression half cycle [22, 24]. In sonochemistry, the reaction proceeds from the bubble interior to the bubble wall (comprising a vapor-liquid interface) to the surrounding liquid. For a reactant mixture, the bubble interior consists of solvent and solute vapors. If a non-volatile solvent is used, the presence of solute vapors can be achieved inside the bubble thus maintaining the reaction within the bubble [5]. Vapors continue to diffuse into the bubble during the growth phase of the bubble from the adjacent liquid. For nanoparticle chemistries, particles have been found to nucleate within bubbles [25] in a process called sonocrystallization [26].

Bubble nucleation, growth and cavitation are the primary phenomena occurring within the continuous reactor. In order to reduce the internal volume of the reactor the critical dimension has to be significantly larger than the critical bubble size at cavitation. This ensures constant

outflow without pressure buildup within the reactor. To evaluate this, a high speed camera (Phantom Miro, Wayne, NJ, USA) was used to capture the stages in bubble cavitation directly below the high intensity ultrasound horn. The images were captured at 60,000 frames per second to capture a phenomenon occurring based on the input of 20 kHz ultrasonic energy. Figure 4 shows the high speed images and the various stages can be observed, at bubble nucleation stage it appears spherical. As the rarefaction part of the ultrasound couples with the bubble it stretches and grows. There is an alternation between growth and shrinkage with overall growth occurring. Finally as the bubble reaches a critical diameter it implodes. The bubble diameter during the growth phase was found to be less than 150 μm. This finding matches with that observed by Suslick et al [24].

Figure 4. Bubble growth dynamics in various stages during acoustic cavitation

4. Results and discussion

Experiments were carried out by fixing the concentrations of the reactant in batch mode with constant amplitude. In continuous mode, flow rate was fixed at 10 ml/min net flow rate. Figure 5 summarizes the TEM results obtained for the nanoparticles during batch synthesis at a) one hour and b) two hours. At one hour, a mixture of very small amorphous particles, ordering less than 10 nm, along with large chunks of nanoparticles ordering 250 nm, were observed. The small particles correspond to freshly formed nuclei which is apparent from their amorphous nature as observed from the weak contrast from the TEM images. At two hours, we can see a wide distribution of irregular shaped particles. This shows higher conversion of the reactants owing to the presence of higher fraction of particles. It is also apparent that the particle size distribution is wide ranging from 50 nm to 200 nm suggesting poor process control.

Figure 5. Particle morphology of CdS in batch sonochemical synthesis. It can be seen from comparison between left and right images there exists at least a bimodal distribution in particle size

The same chemistry was run through the sonochemical flow cell. Under experimental conditions, the mixed reactants were exposed for a fluid residence time of 48 seconds at an average power of 100 W. The fluid temperature inside the flow cell rose at a rate of ~50°C/min. When the fluid reached a reaction temperature of 85°C, the outflow was found to be pale yellow in color which is characteristic of a suspension containing cadmium sulfide. The cadmium sulfide nanoparticles were collected and quenched in a vial to stop the reaction and then imaged using the TEM. The corresponding images are shown in Figure 6a. It is apparent the predominant morphology of samples is hexagonal platelets collected at various points after onset of steady state (SS) and 3 minutes and 6 minutes after onset of SS. As observed in the micrographs, the contrast of underlying platelets suggests that the platelets are thin. Figure 6b shows the particle size distribution of the corresponding images. The distributions are nearly Gaussian with a predominant skewing to the left that shifts the mean. The corresponding mean particle sizes are listed in Table 3. As shown, the average sizes of the particles are very close with similar standard deviations. A Tukey multiple comparison test [27] shows there is no significant difference between the particle size distribution at 3 and 6 minutes. The coefficient of variation (CV) at 3 and 6 minute shows good process control with CVs similar to those previously reported.

(a)

(b)

Figure 6. Particle morphology of CdS in continuous synthesis a)Transmission electron micrographs b) corresponding particle size distributions

Table 3. Particle size statistics for CdS NPs synthesized via continuous sonochemistry

	SS	SS + 3 min	SS + 6 min
Avg size (nm)	19.3	21.3	22.9
SD (nm)	6.2	5.2	5.8
CV %	32.6%	24.3%	25.2%

In another experiment, samples collected at steady state were quenched with various delays to check the progress of the reaction with time after the particles leave the sonochemical reactor. Figure 7 shows the particle morphology and distribution as a function of quench delay time.

(a)

(b)

Figure 7. a) Change in CdS NP morphology as a function of quench delay and b) corresponding particle size distribution

An interesting morphological evolution occurs upon observing the TEM images. NPs quenched after 15 minutes from collection still retain hexagonal platelet shape while at 30 minutes the particle edges appear to get rounded or smooth. The faceted appearance starts to disappear and is completely absent when quenching is delayed by one hour where in the particles appear to be well rounded or nearly spherical. It is also interesting to note that the shape of the particle size distribution in Figure 7b does not change with quench delay suggesting that the distribution follows the same trend with time. The corresponding mean sizes are listed in Table 4.

Table 4. Effect of quench delay on mean particle size

Quench delay	15 min	30 min	60 min
Avg size (nm)	31.7	21.7	12.5
SD (nm)	11.1	4.9	5.1
CV %	35.2	22.7	40.8

From Table 4, it is apparent that the NP average size is decreasing with quench delay time. This suggests that another particle growth mechanism is active instead of the classical Ostwald ripening. One reason that the average size is decreasing is because the particle morphology changes from a high aspect ratio platelet to a spherical particle. Since volume has to be conserved, the average particle size decreases. This rearrangement of particle shape and size could occur by surface diffusion of Cd and S ions around the particles. To evaluate the thickness of the nanoparticle platelets the product sampled after 6 minutes from steady state were used to form a thin film on a silicon substrate. On the as-coated sample, a carbon coating was deposited for contrast and a chromium layer was deposited for protecting the top surface of the film from the focused ion beam used to section the sample. A thin section of approximately 15 um x 5 um x 0.25 um sampling a cross section of the nanoparticle film and the silicon substrate was cut. Subsequently this section was further polished in the ion beam and observed under the TEM for finding the dimension of the nanoparticles in the thickness direction and is shown in Figure 8.

Figure 8. Cross sectional TEM image showing differentiation in contrast from various layers and zoomed areas showing structure

It can be easily observed that the CdS nanoparticle layer is 10 nm thick and within this layer sub 10 nm features could be discerned suggesting that the 22 nm hexagonal platelets have a thickness less than 10 nm. In order to validate whether the hexagonal platelets could be formed only in the sonochemical route a study using conventional heating using a hot plate for the same chemistry

was performed. Yellow precipitates were formed and were prepared for subsequent TEM examination. The results are shown in Figure 9 below.

Figure 9. Particle morphology of CdS in batch conventional heating induced synthesis

It can be observed that the particle size varies from about 20 nm to 0.5 µm after one hour of synthesis and varies from about 20 nm to one µm after two hours of synthesis. It is obvious that the size dispersion is very poor and it is notable that there are no hexagonal-shaped particles. Even after two hours of synthesis it can be seen that there are long strands of unreacted thiourea spanning several µm as seen from bottom left image in Figure 9. This shows that hexagonal-shaped CdS nanoparticles are observed only in the sonochemical route and to a higher degree in the continuous mode.

Phase identification was carried out using x-ray diffraction on the CdS chemistry wherein different heating modes were compared as shown in Figure 10 below.

Hex CdS		Cubic CdS		Thiourea	
l	(100)	a	(111)	x	(120)
m	(002)	b	(200)	y	(022)
n	(101)	c	(220)	z	(200)
o	(110)	d	(311)		
p	(200)				
q	(112)				

Figure 10. Identification of CdS nanoparticle crystal structure using X-ray diffraction [BTHT – Batch conventional heating, Bat – Batch ultrasound induced heating, SS - Onset of steady state in continuous ultrasound heating]. Corresponding index table is shown for the various phases.

From the XRD results, it can be observed that cubic CdS peaks are predominantly present in continuous mode when compared to batch synthesis where majority of the peaks belong to

hexagonal CdS. The patterns were indexed using standards 80-0006 for hexagonal CdS and 89-0440 for cubic CdS in conjunction with ICDD PDF-2 database. In batch ultrasound heating, we can observe a mixture of cubic and hex CdS peaks. However, in conventional heating, it can be observed that all the CdS peaks are of hexagonal crystal structure and there are no cubic CdS peaks. It is also noted that there are thiourea peaks present in the batch conventional synthesis mode and that the thiourea peaks reduce in number with increasing synthesis temperature suggesting that the reaction is incomplete in general.

These results suggest that the metastable cubic CdS is difficult to achieve in conventional heating of the same chemistry. The presence of cubic CdS in ultrasound-induced reactions suggests that it is caused by the high temperatures that are possible in sonochemical reaction. Bubble implosion during sonication has been estimated to increase the local temperature of the surrounding liquid to over 5000°C and increase the local pressure to nearly 1000 atm [28, 29]. Such effects have been observed by others experimentally [30].

Several factors influence the crystal structure of CdS particles, though the key factors are the sources of cadmium and sulfur. In general when sodium sulfide is used as a reactant, it entails formation of cubic CdS even with various Cd sources while usage of organic sulfur sources (thio groups) generally result in formation of mixture of cubic and hexagonal phases of CdS [31]. In sonochemical synthesis, the structure is also affected by the intensity and type (dispersed vs. intense) of sonication used. Also solvation of the reagents and interfacial forces for various kinds of Cd salt solutions affect structure [11]. Typical vapor phase methods for production of high aspect ratio particles (belts, tubes and wires) involve temperatures above 800°C [32] and result in formation of hexagonal CdS. Cubic CdS is reported to be a metastable phase [33] as opposed to hexagonal CdS and reverts to this structure upon heating to temperatures above 300°C [34]. In this case, the continuous sonochemical synthesis of CdS appears to have stabilized the cubic phase within high aspect ratio nanoplatelets. It is to be noted that typical microwave synthesis i.e. another high energy rapid heating technique yields hexagonal CdS particles [35].

Further, large-format compositional sampling of approx 4 μm^3 was performed using wavelength dispersive spectroscopy (WDS) to look at compositional homogeneity in the precipitates. Results

are summarized in Figure 11. The data for this summary plot is shown in Table 5 and the raw data is shown in appendix 1, Table 6.

Figure 11. Compositional homogeneity shown as atomic % ratio of Cd to S in various samples [BHT – Batch conventional heating, BAT – Batch ultrasound heating, SS – Continuous ultrasound heating at steady state]

Table 5: WDS atomic % values measured on various CdS samples.

Synthesis mode	S (at %)	Cd (at %)	Cd/S atomic ratio
BHT120 min	17.26	82.85	4.80
BHT60 min	8.10	90.81	11.21
BAT120 min	6.96	92.42	13.28
BAT60 min	5.80	91.11	15.70
SS	34.93	63.24	1.81
SS+3 min	47.02	48.42	1.03
SS+6 min	30.82	68.10	2.21

Upon examining the above results, it can be noted that for the steady state continuous synthesis the atomic ratio is very close to the expected 1:1 for Cd:S within the standard error limits. For conventional heating the ratio is much greater than one while in batch ultrasound it is even worse showing very high cadmium concentration. In both cases, the Cd:S ratio is improving with time suggesting that the reactions are incomplete even after two hours. This is congruent to what was observed in the XRD results showing the presence of unreacted thiourea. This confirms that the continuous sonochemical synthesis is much faster. One explanation for this could be well mixed reagents prior to the continuous reactor.

5. Conclusions

Continuous sonochemical synthesis was found to be capable of producing a metastable phase of CdS in the form of high aspect ratio platelets. The phase and shape of the nanoplatelets provide evidence of high reaction temperatures. Relative to the other processes investigated in this study, continuous sonochemical synthesis provides an eightfold reduction in processing time of the product while exhibiting good size and compositional control. At steady state, the size of the

hexagonals averaged 21.0 nm in diameter with an average coefficient of variation of 27.4%. The thickness of the nanoplatelets was found to be less than 10 nm opening the possibility of quantum confinement and application as quantum wells.

6. Acknowledgements

The work described here was funded by the US Department of Energy, Industrial Technologies Program, through award #NT08847, under contract DE-AC-05-RL01830. Additional funds were received from the Oregon Nanoscience and Microtechnologies Institute (ONAMI) under a matching grant to Oregon State University. The facilities and equipment resident at the Microproducts Breakthrough Institute (MBI) and the Oregon Process Innovation Center (OPIC) were used in conducting this study. The authors would also like thank Mr. Neill Thornton (MBI) for his help in performing high speed photography and Dr Peter Eschbach for his help in the focused ion beam milling technique.

7. References

[1] C. Engelbrecht, Electricity from the Sun, Quest, 2 (2006) 8-10.
[2] H. Moualkia, S. Hariech, M.S. Aida, N. Attaf, E.L. Laifa, Growth and physical properties of CdS thin films prepared by chemical bath deposition, Journal of Physics D: Applied Physics, 42 (2009) 135404.
[3] V.I. Klimov, Nanocrystal Quantum Dots, Second Edition, Taylor and Francis, 2009.
[4] S. Kar, S. Chaudhuri, Cadmium sulfide one-dimensional nanostructures: Synthesis, characterization and application, Synthesis and Reactivity in Inorganic, Metal-Organic, and Nano-Metal Chemistry, 36 (2006) 289-312.
[5] Y. Mastai, A. Gedanken, Sonochemistry and Other Novel Methods Developed for the Synthesis of Nanoparticles, ChemInform, 37 (2006) no-no.
[6] D.A. Peterson, P. Chandran, B.K. Paul, A Reverse Oscillatory Flow microreactor system for the synthesis of uniformly-size CdS nanoparticles, in: Nanotechnology (IEEE-NANO), 2011 11th IEEE Conference on, IEEE, 2011, pp. 666-670.
[7] Z. Wan, H.W. Yang, W.L. Luan, S.T. Tu, X.G. Zhou, Facile Synthesis of Monodisperse CdS Nanocrystals via Microreaction, Nanoscale Research Letters, 5 (2010) 130-137.
[8] G.Z. Wang, Y.W. Wang, W. Chen, C.H. Liang, G.H. Li, L.D. Zhang, A facile synthesis route to CdS nanocrystals at room temperature, Materials Letters, 48 (2001) 269-272.
[9] G.S. Wu, X.Y. Yuan, T. Xie, G.C. Xu, L.D. Zhang, Y.L. Zhuang, A simple synthesis route to CdS nanomaterials with different morphologies by sonochemical reduction, Materials Letters, 58 (2004) 794-797.
[10] T. Gao, Q. Li, T. Wang, Sonochemical Synthesis, Optical Properties, and Electrical Properties of Core/Shell-Type ZnO Nanorod/CdS Nanoparticle Composites, Chemistry of Materials, 17 (2005) 887-892.

[11] N. Ghows, M. Entezari, A novel method for the synthesis of CdS nanoparticles without surfactant, Ultrasonics Sonochemistry, 18 (2011) 269-275.
[12] H. Wang, Y. Luf, J. Zhu, Preparation of Cube-Shaped CdS Nanoparticles by Sonochemical Method, in, World Scientific Pub Co Inc, 2003, pp. 63.
[13] S.F. Wang, F. Gu, M.K. Lü, Sonochemical synthesis of hollow PbS nanospheres, Langmuir, 22 (2006) 398-401.
[14] R. Xie, D. Li, D. Yang, M. Jiang, Surface synthesis of PbS nanoparticles on silica spheres by a sonochemical approach, Journal of Materials Science, 42 (2006) 1376-1380.
[15] T. Banert, C. Horst, U. Kunz, U. Peuker, Continuous precipitation in an ultrasonic flow reactor as illustrated by iron(II, III) oxide, Chem. Ing. Tech., 76 (2004) 1380-1381.
[16] T. Banert, G. Brenner, U.A. Peuker, Operating parameters of a continuous sono-chemical precipitation reactor, Proc. 5. WCPT, Orlando, Fl, (2006) 23-27.
[17] T.J. Mason, J. Phillip, Applied sonochemistry, Wiley-VCH Weinheim, Germany, 2002.
[18] K. Yasui, Y. Iida, T. Tuziuti, T. Kozuka, A. Towata, Strongly interacting bubbles under an ultrasonic horn, Physical Review E, 77 (2008) 016609.
[19] P.H. Mugdur, Y.J. Chang, S.Y. Han, Y.W. Su, A.A. Morrone, S.O. Ryu, T.J. Lee, C.H. Chang, A Comparison of Chemical Bath Deposition of CdS from a Batch Reactor and a Continuous-Flow Microreactor, Journal of The Electrochemical Society, 154 (2007) D482-D488.
[20] Y.J. Chang, Y.W. Su, D.H. Lee, S.O. Ryu, C.H. Chang, Investigate the Reacting Flux of Chemical Bath Deposition by a Continuous Flow Microreactor, Electrochemical and Solid-State Letters, 12 (2009) H244-H247.
[21] F.A. Bettelheim, W.H. Brown, M.K. Campbell, S.O. Farrell, O.J. Torres, Introduction to organic and biochemistry, Thomson Brooks/Cole, 2012.
[22] A. Colussi, L.K. Weavers, M.R. Hoffmann, Chemical bubble dynamics and quantitative sonochemistry, The Journal of Physical Chemistry A, 102 (1998) 6927-6934.
[23] R. van Eldik, C.D. Hubbard, Chemistry under extreme and non-classical conditions, Wiley, 1996.
[24] K.S. Suslick, D.J. Flannigan, Inside a collapsing bubble: sonoluminescence and the conditions during cavitation, Annu. Rev. Phys. Chem., 59 (2008) 659-683.
[25] R. Chow, R. Blindt, R. Chivers, M. Povey, A study on the primary and secondary nucleation of ice by power ultrasound, Ultrasonics, 43 (2005) 227-230.
[26] M. Luque de Castro, F. Priego-Capote, Ultrasound-assisted crystallization (sonocrystallization), Ultrasonics Sonochemistry, 14 (2007) 717-724.
[27] J. Tukey, J. Ciminera, J. Heyse, Testing the statistical certainty of a response to increasing doses of a drug, Biometrics, (1985) 295-301.
[28] K.S. Suslick, G.J. Price, Applications of ultrasound to materials chemistry, Annual Review of Materials Science, 29 (1999) 295-326.
[29] K. Suslick, M. Fang, T. Hyeon, M. Mdleleni, Applications of sonochemistry to materials synthesis, Kluwer Publishers: Dordrecht, Netherlands, 1999.
[30] E. Ciawi, J. Rae, M. Ashokkumar, F. Grieser, Determination of temperatures within acoustically generated bubbles in aqueous solutions at different ultrasound frequencies, The Journal of Physical Chemistry B, 110 (2006) 13656-13660.
[31] Z. Fu, S. Zhou, J. Shi, S. Zhang, Effects of precursors on the crystal structure and photoluminescence of CdS nanocrystalline, Materials Research Bulletin, 40 (2005) 1591-1598.
[32] T. Zhai, X. Fang, L. Li, Y. Bando, D. Golberg, One-dimensional CdS nanostructures: synthesis, properties, and applications, Nanoscale, 2 (2010) 168-187.

[33] S. Gorer, G. Kodes, Y. Sorek, R. Reisfeld, Crystal phase transformation in sol-gel films of nanocrystalline CdSe and CdS, Materials Letters, 31 (1997) 209-214.
[34] L. Wan, Z. Bai, Z. Hou, D. Wang, H. Sun, L. Xiong, Effect of $CdCl_2$ annealing treatment on thin CdS films prepared by chemical bath deposition, Thin Solid Films, 518 (2010) 6858-6865.
[35] R. Amutha, M. Muruganandham, G. Lee, J. Wu, Facile Microwave-Combustion Synthesis of Wurtzite CdS Nanoparticles, Journal of Nanoscience and Nanotechnology, 11 (2011) 7940-7944.

Appendix 1

Table 6. Raw compositional data from WDS scans

BHT 120 min		BHT 60 min		BAT 120 min		BAT 60 min		SS		SS + 3 min		SS + 6 min	
Atomic%		Atomic%		Atomic%		Atomic%		Atomic%		Atomic%		Atomic%	
S	Cd	S	Cd	S	Cd	S	Cd	S	Cd	S	Cd	S	Cd
16.03	84.08	2.63	97.04	6.62	92.72	5.78	90.91	38.61	60.14	45.92	44.58	31.82	67.42
16.21	83.82	9.91	89.83	7.62	91.65	5.55	91.44	33.81	64.74	49.09	48.17	32.23	65.21
18.02	82.12	9.17	90.25	6.57	93.07	5.60	91.58	35.53	62.75	45.62	52.54	30.27	69.17
18.78	81.36	7.08	92.57	7.36	92.00	6.27	90.71	34.26	63.83	47.50	49.32	30.26	69.04
10.99	89.03	7.38	92.05	7.21	92.12	5.73	91.00	33.72	64.46	47.91	46.63	31.82	67.42
		8.56	91.35	7.13	92.41	5.78	91.10	37.31	60.43	46.23	46.40	29.76	69.18
		7.62	86.12	6.68	92.65	5.50	91.34			48.76	49.21	29.58	69.24
		2.32	97.63	6.88	92.68	6.02	91.07			45.16	50.51		
		7.33	92.61	6.76	92.27	5.92	91.01						
		7.76	91.69	6.76	92.64	5.87	90.94						
		1.25	98.76			5.80	91.11						

Table 1. Nanoparticle size distributions reported in the literature

Material	Avg Size (nm)	SD (nm)	CV (%)	Synthesis Approach	Author
CdSe	8.0	0.6	8.0	Sonochem	Mastai et al [5]
CdSe	3.0	0.6	19.7	Sonochem	Mastai et al [5]
CdSe	4.0	0.7	17.0	Sonochem	Mastai et al [5]
CdSe	5.5	0.6	10.2	Sonochem	Mastai et al [5]
CdS	4.5	1.0	22.2	Microfluidic reactor	Peterson et al [6]
CdS	5.2	0.3	6.0	Microfluidic reactor	Wan et al [7]
CdS	5.5	0.9	16.4	Sonochem*	Wang et al [8]
CdS	11.5	6.5	56.3	Sonochem*	Wu et al [9]
CdS	8.5	3.5	40	Sonochem*	Gao et al [10]

Table 2. Experimental conditions for sonochemical synthesis of CdS

Parameters	Batch	Continuous
Chemistry	$CdCl_2$ + $CS(NH_2)_2$ + NH_4Cl + NH_4OH	$CdCl_2$ + $CS(NH_2)_2$ + NH_4Cl + NH_4OH
Processing time	120 min	48 sec
Reynolds no	-	410
Ultrasound Power (Avg)	20 W	100 W

Table 3. Particle size statistics for CdS NPs synthesized via continuous sonochemistry

	SS	SS + 3 min	SS + 6 min
Avg size (nm)	19.3	21.3	22.9
SD (nm)	6.2	5.2	5.8
COV %	32.6%	24.3%	25.2%

Table 4. Effect of quench delay on mean particle size

Quench delay	15 min	30 min	60 min
Avg size (nm)	31.7	21.7	12.5
SD (nm)	11.1	4.9	5.1
COV %	35.2	22.7	40.8

Table 5: WDS atomic % values measured on various CdS samples

Synthesis mode	S (at %)	Cd (at %)	Cd/S atomic ratio
BHT120 min	17.26	82.85	4.80
BHT60 min	8.10	90.81	11.21
BAT120 min	6.96	92.42	13.28
BAT60 min	5.80	91.11	15.70
SS	34.93	63.24	1.81
SS+3 min	47.02	48.42	1.03
SS+6 min	30.82	68.10	2.21

Table 6. Raw compositional data from WDS scans

BHT 120 min		BHT 60 min		BAT 120 min		BAT 60 min		SS		SS + 3 min		SS + 6 min	
Atomic%		Atomic%		Atomic%		Atomic%		Atomic%		Atomic%		Atomic%	
S	Cd	S	Cd	S	Cd	S	Cd	S	Cd	S	Cd	S	Cd
16.03	84.08	2.63	97.04	6.62	92.72	5.78	90.91	38.61	60.14	45.92	44.58	31.82	67.42
16.21	83.82	9.91	89.83	7.62	91.65	5.55	91.44	33.81	64.74	49.09	48.17	32.23	65.21
18.02	82.12	9.17	90.25	6.57	93.07	5.60	91.58	35.53	62.75	45.62	52.54	30.27	69.17
18.78	81.36	7.08	92.57	7.36	92.00	6.27	90.71	34.26	63.83	47.50	49.32	30.26	69.04
10.99	89.03	7.38	92.05	7.21	92.12	5.73	91.00	33.72	64.46	47.91	46.63	31.82	67.42
		8.56	91.35	7.13	92.41	5.78	91.10	37.31	60.43	46.23	46.40	29.76	69.18
		7.62	86.12	6.68	92.65	5.50	91.34			48.76	49.21	29.58	69.24
		2.32	97.63	6.88	92.68	6.02	91.07			45.16	50.51		
		7.33	92.61	6.76	92.27	5.92	91.01						
		7.76	91.69	6.76	92.64	5.87	90.94						
		1.25	98.76			5.80	91.11						

Figure 1

Click here to download high resolution image

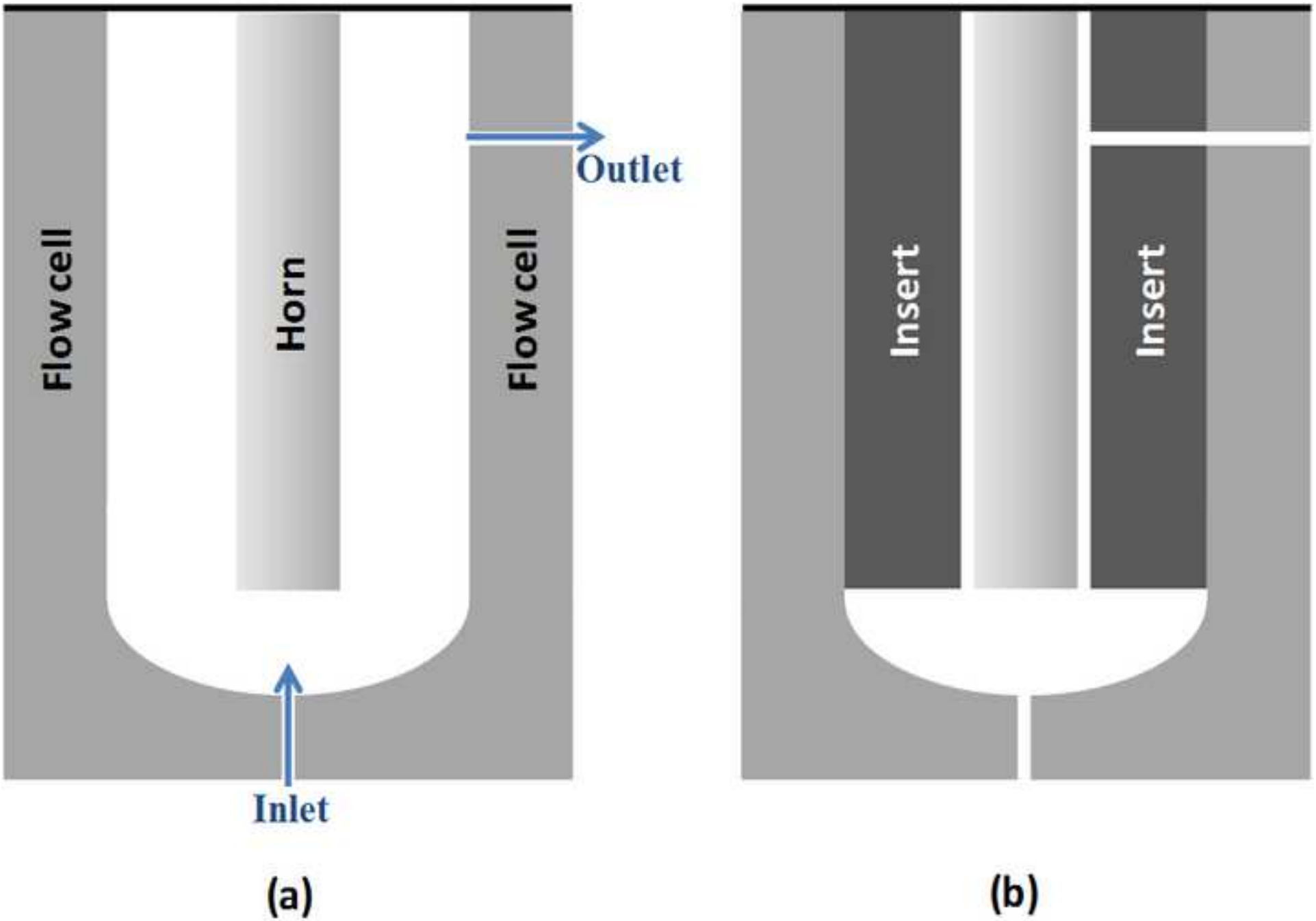

Figure 2

Click here to download high resolution image

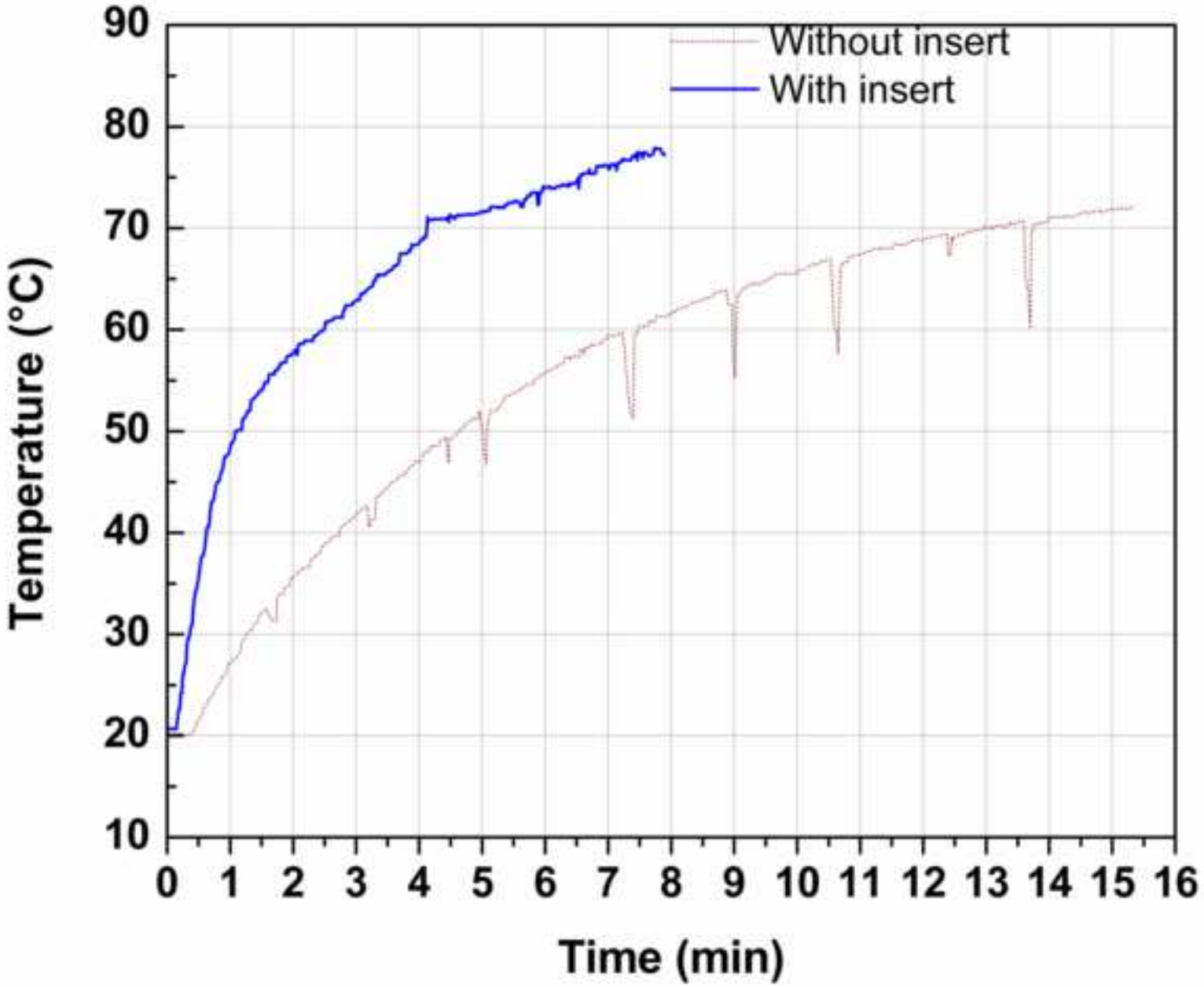

Figure 3

Click here to download high resolution image

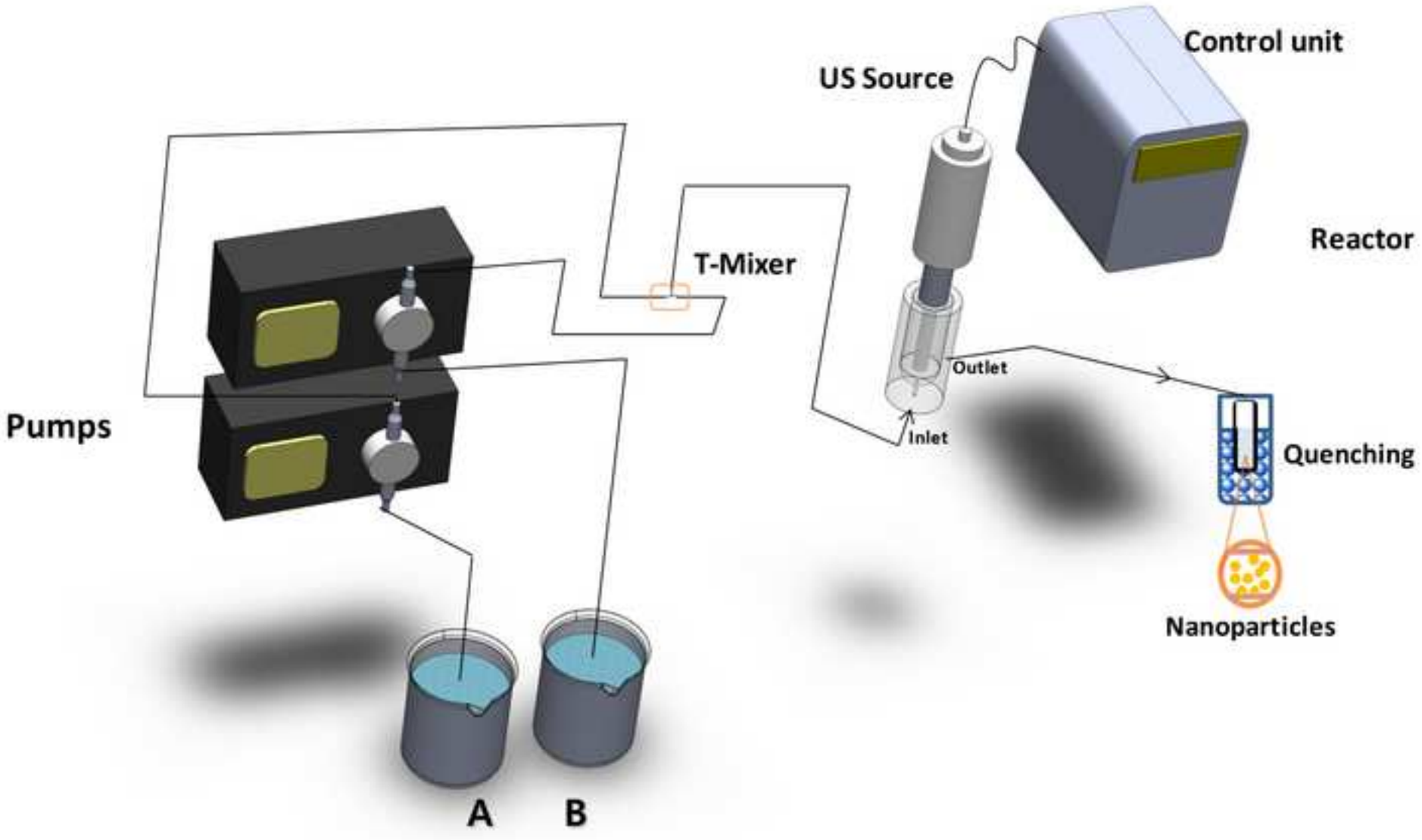

Figure 4

Click here to download high resolution image

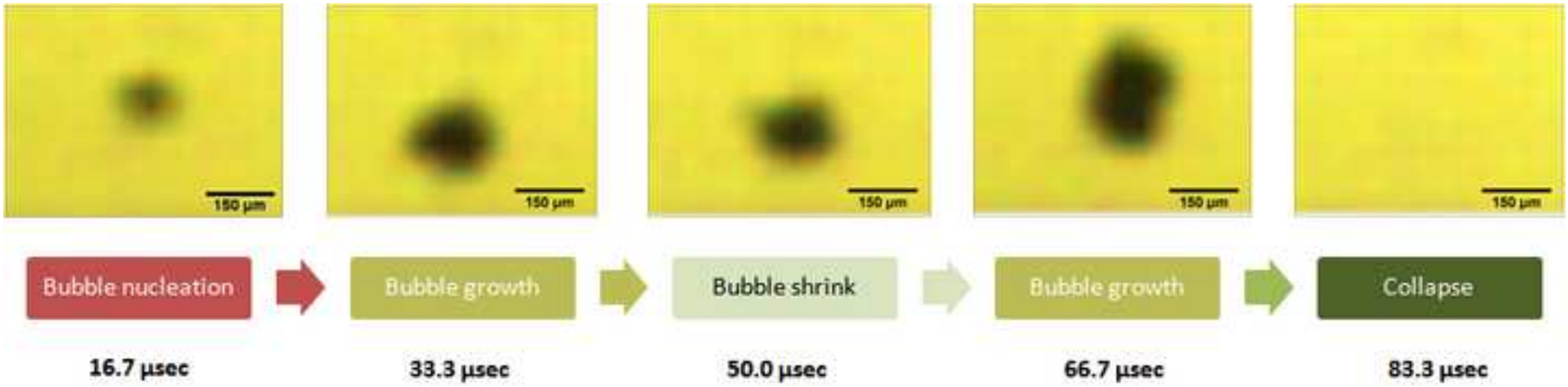

Figure 5

Click here to download high resolution image

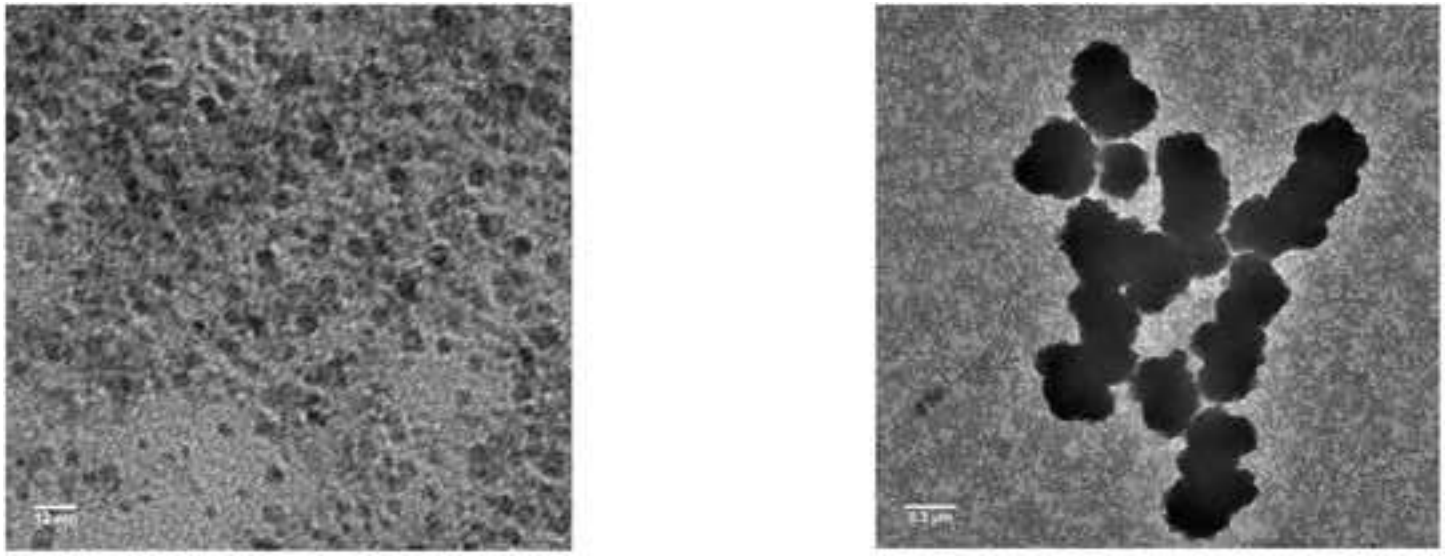

After 1 hr

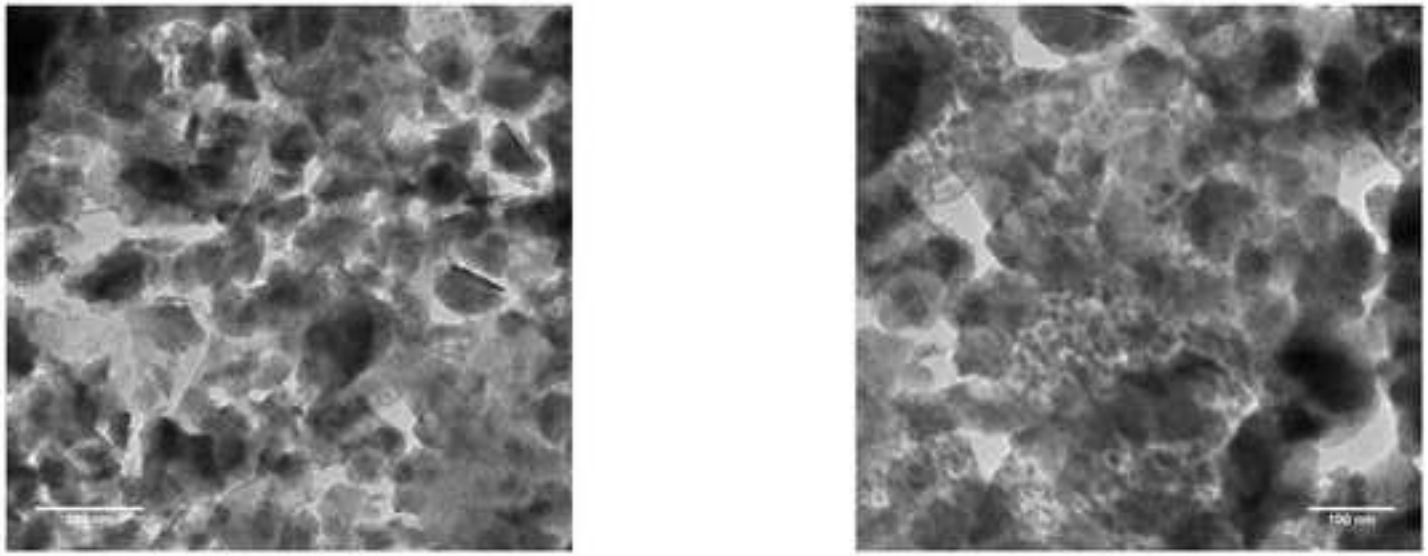

After 2 hr

Figure 6a
Click here to download high resolution image

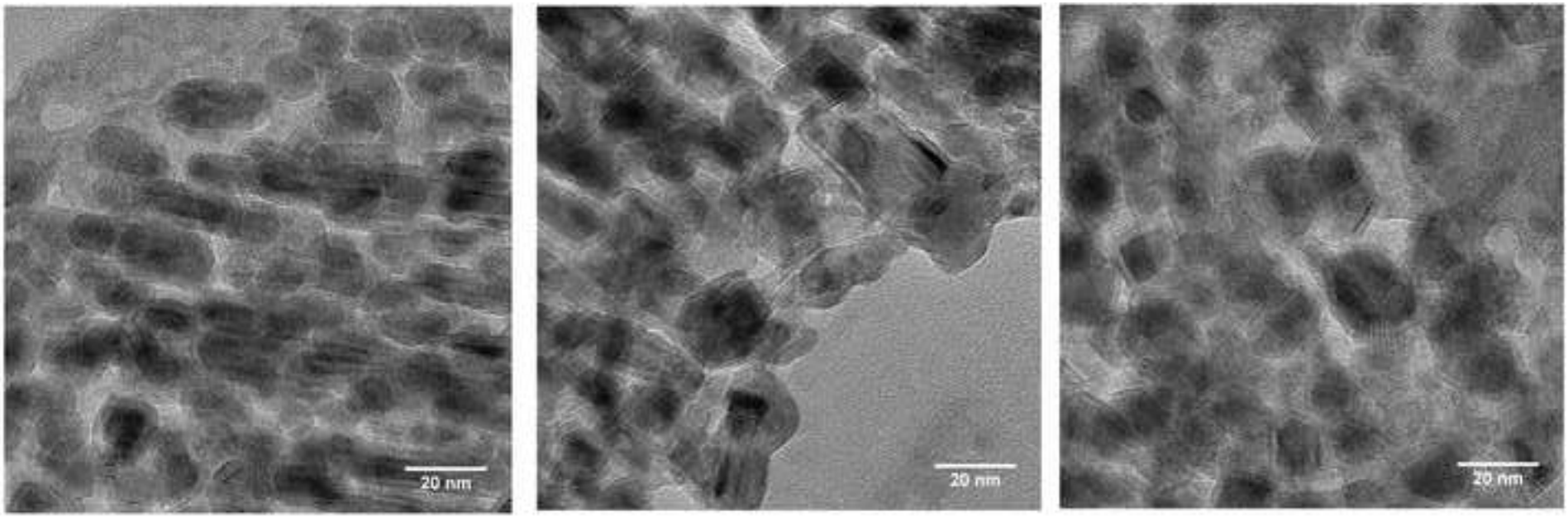

Figure 6b_1
Click here to download high resolution image

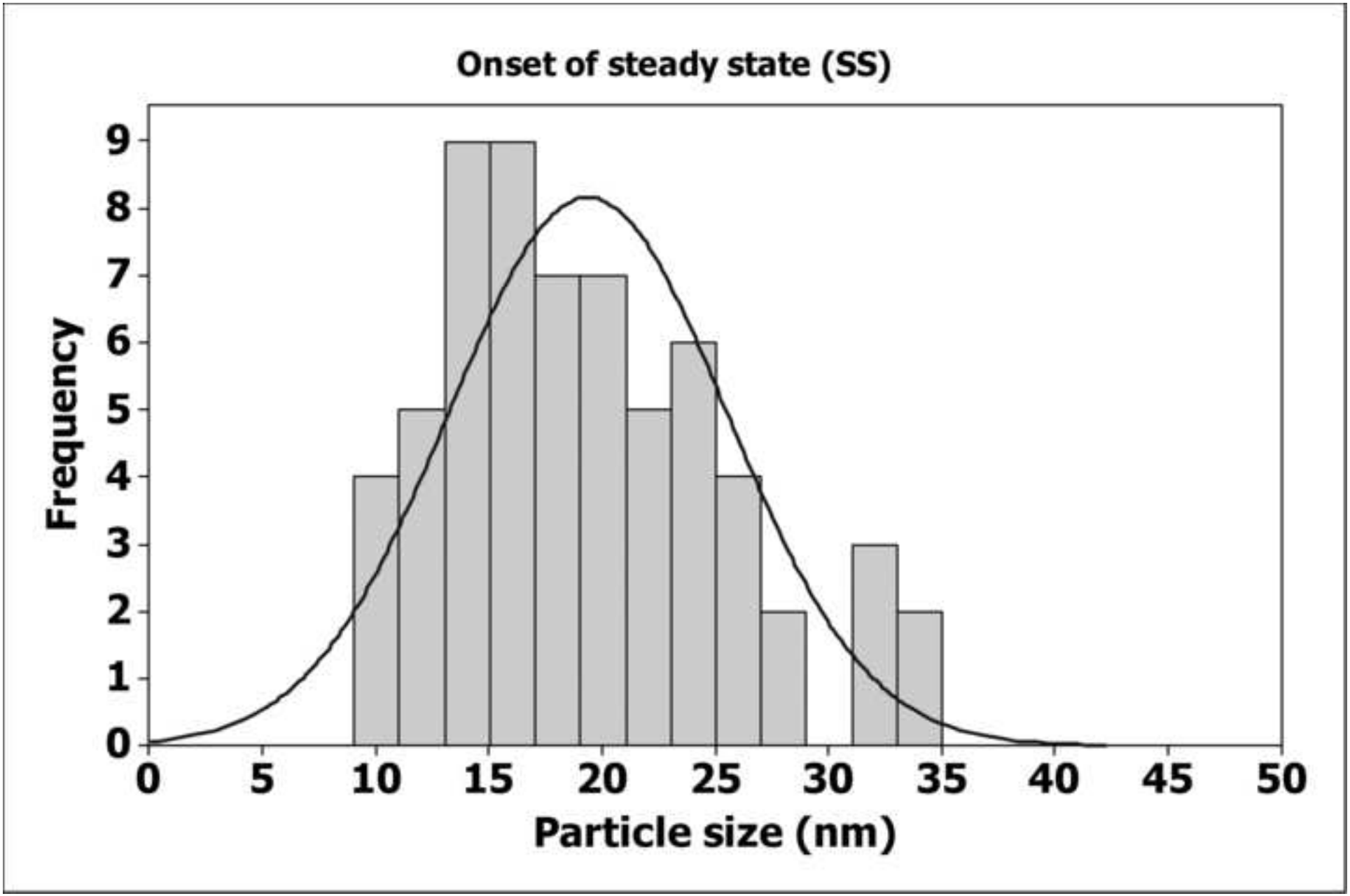

Figure 6b_2
Click here to download high resolution image

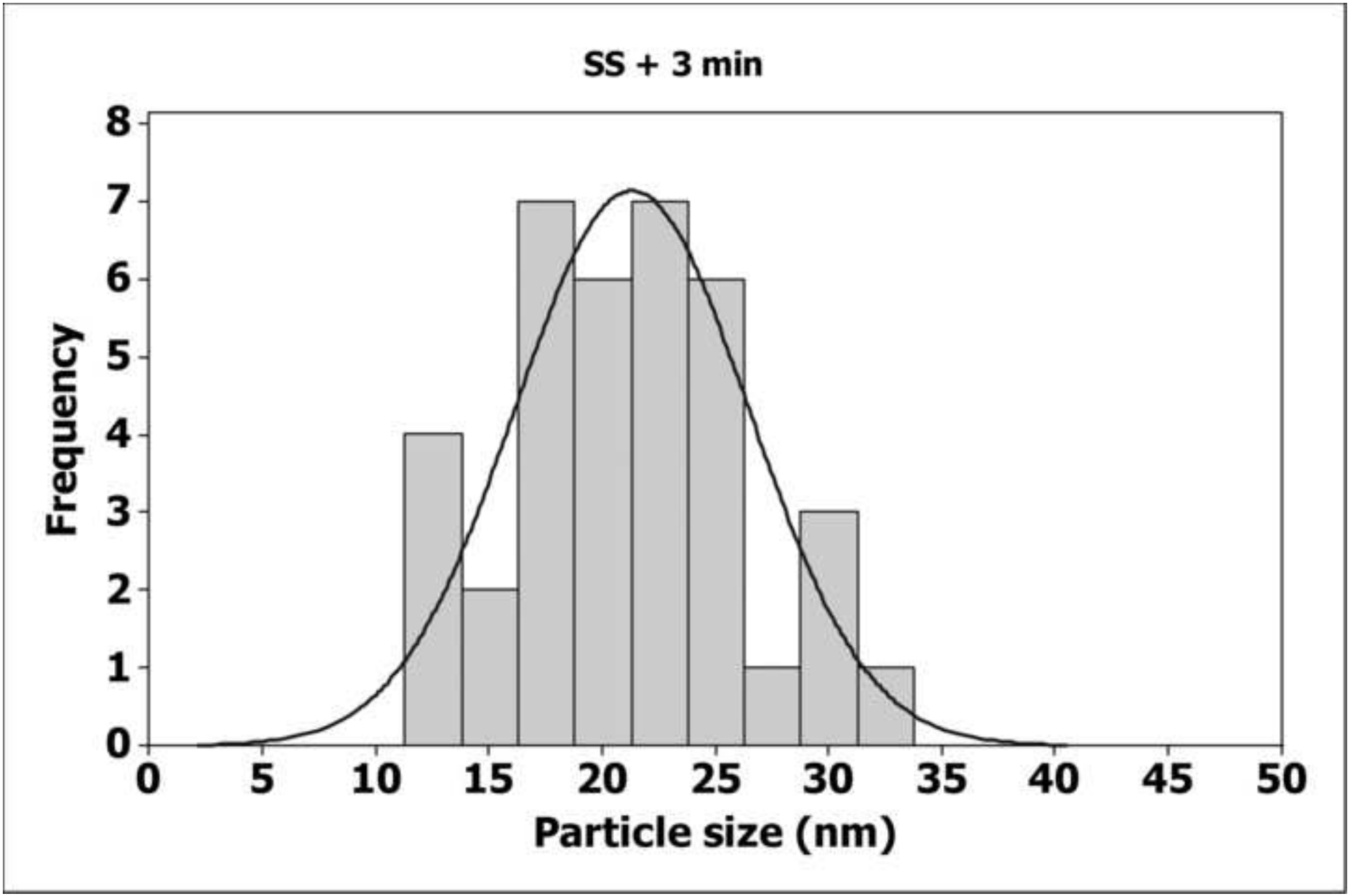

Figure 6b_3
Click here to download high resolution image

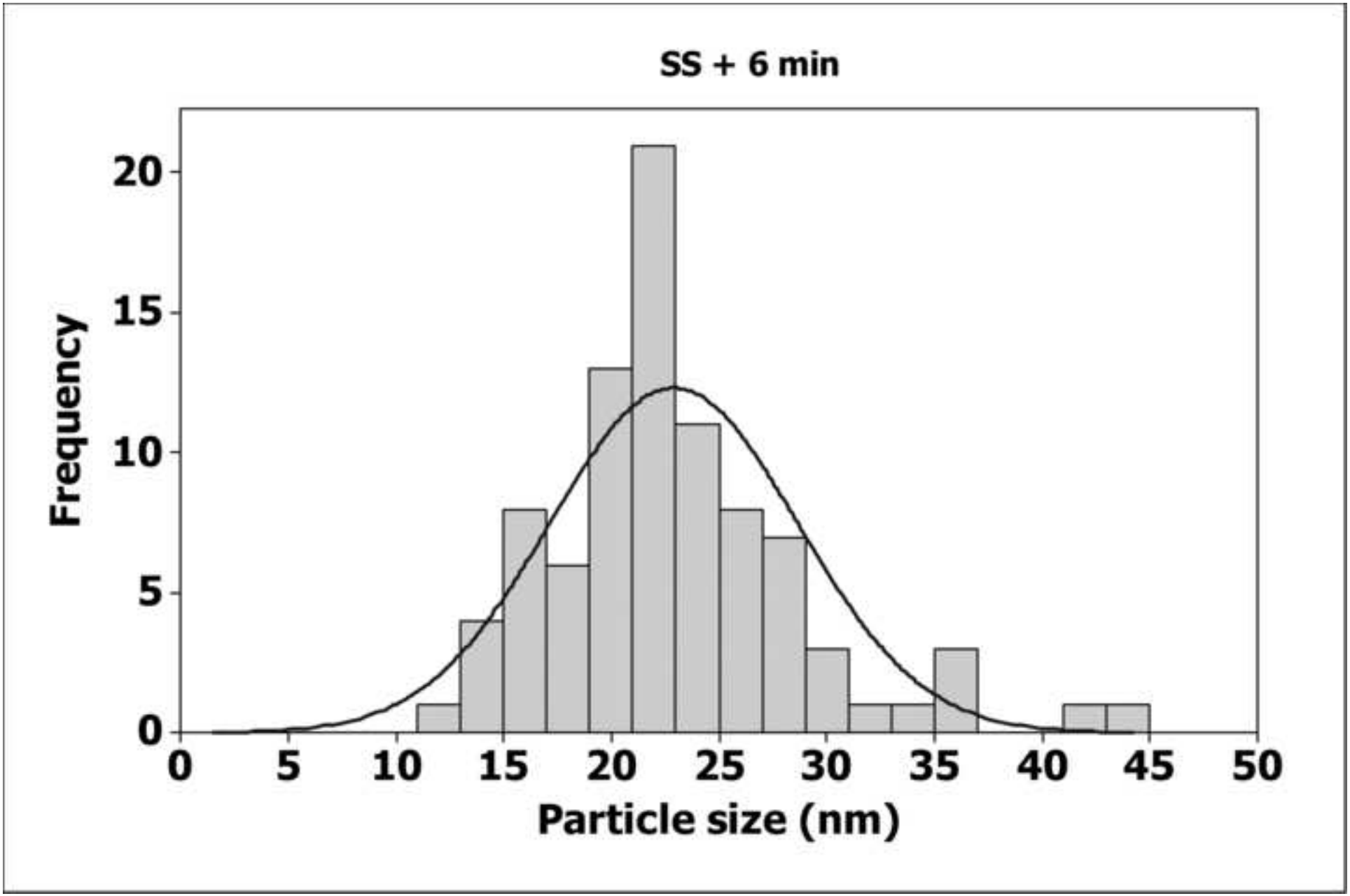

Figure 7a
Click here to download high resolution image

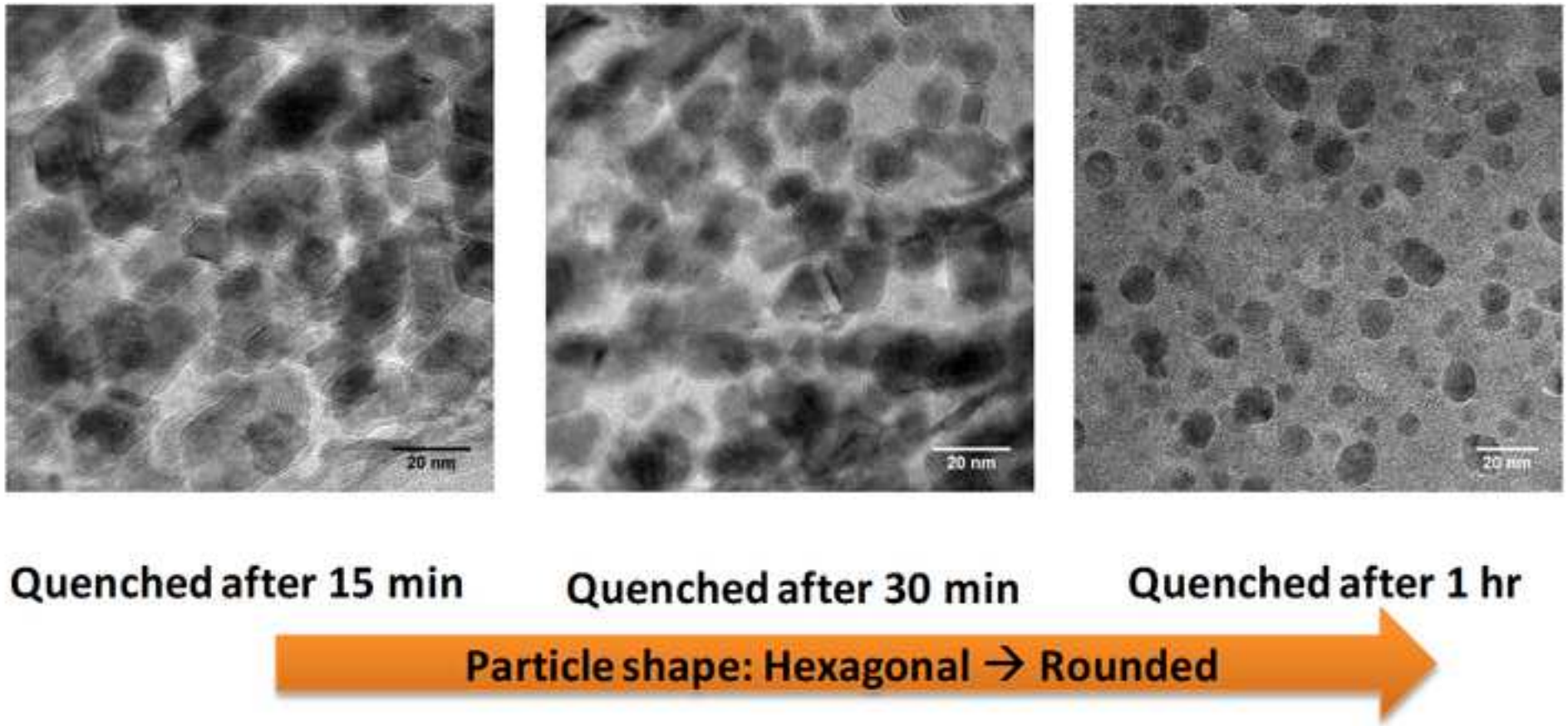

Figure 7b_1
Click here to download high resolution image

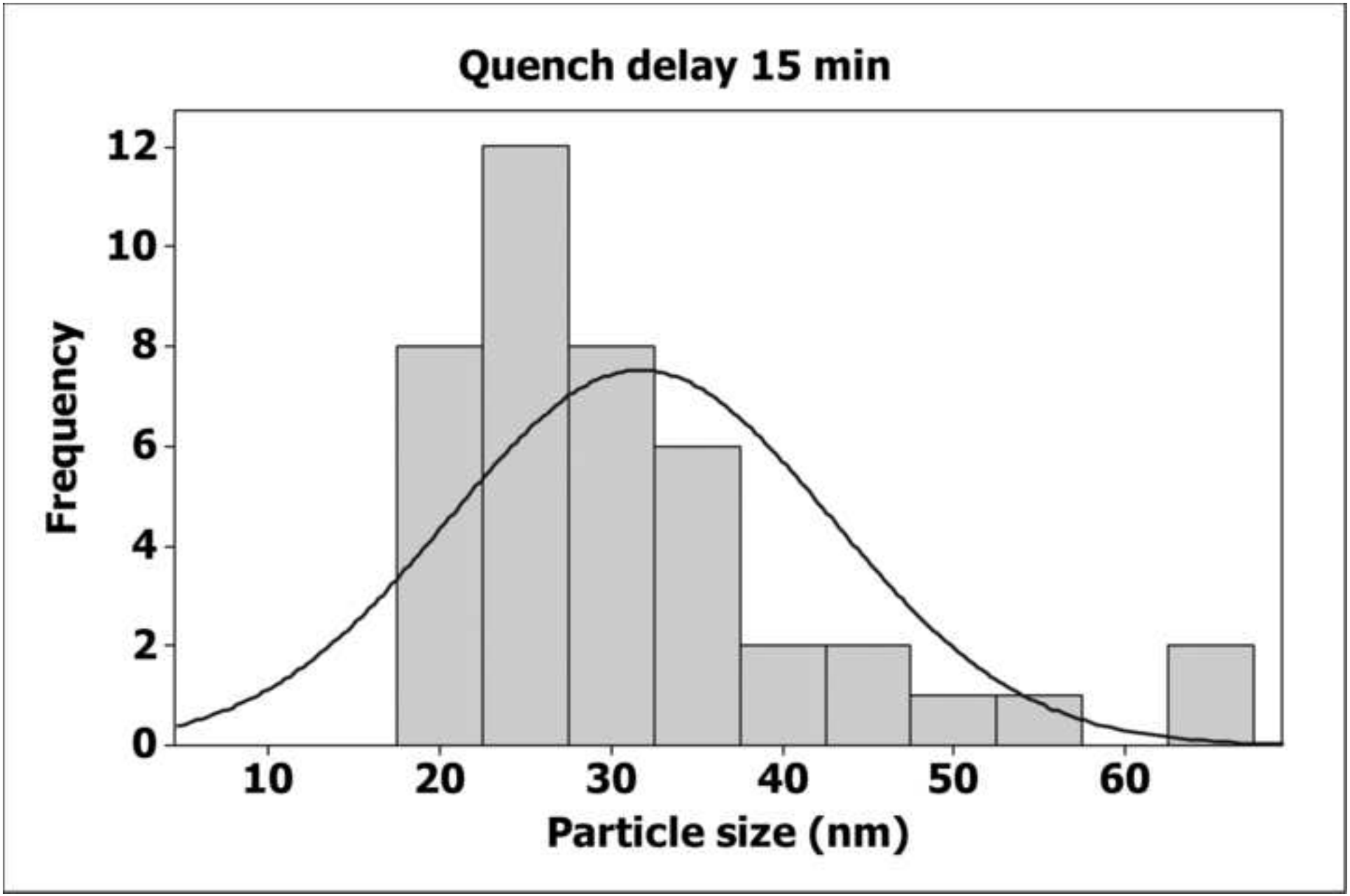

Figure 7b_2
Click here to download high resolution image

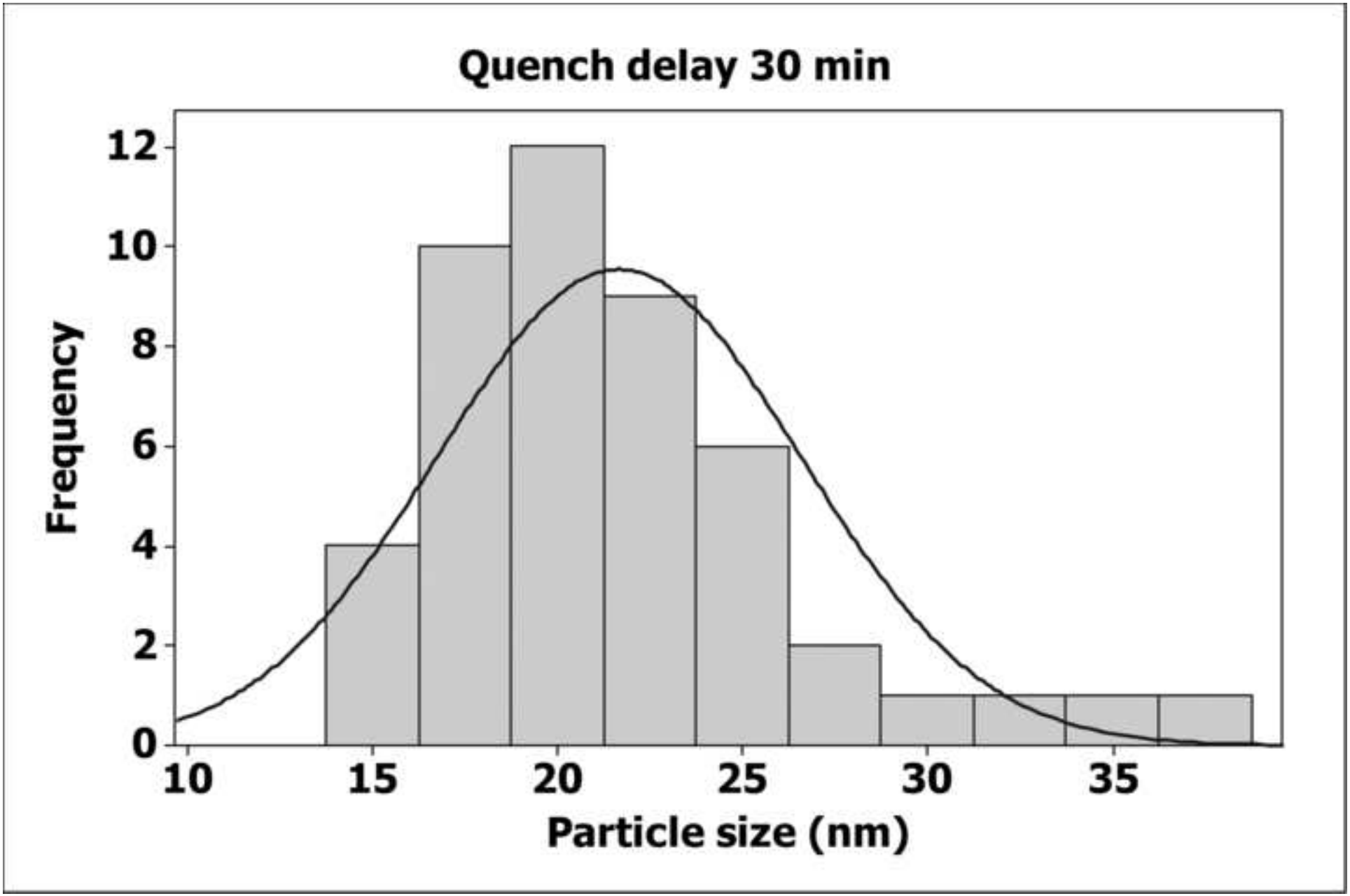

Figure 7b_3
Click here to download high resolution image

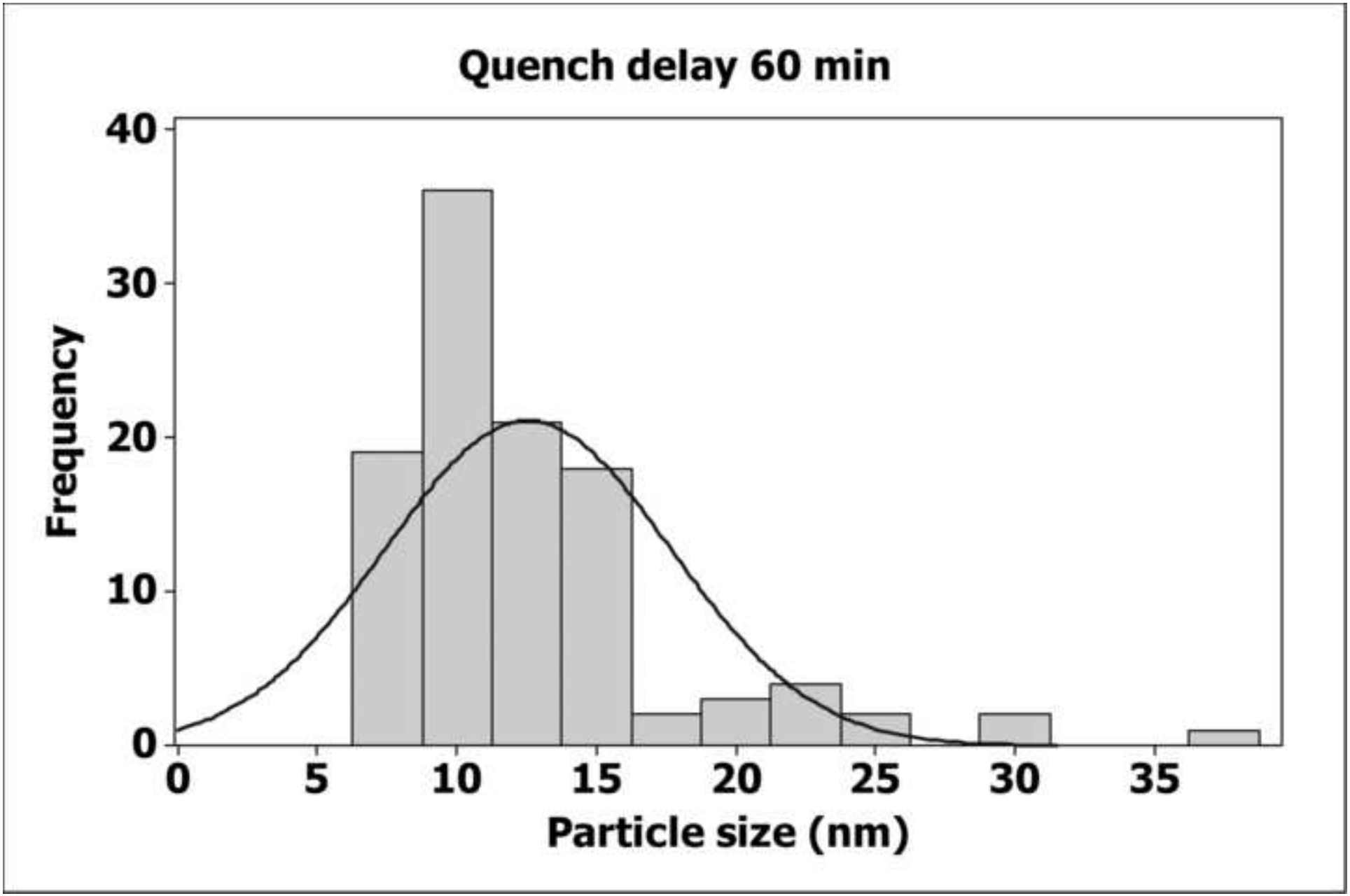

Figure 8
Click here to download high resolution image

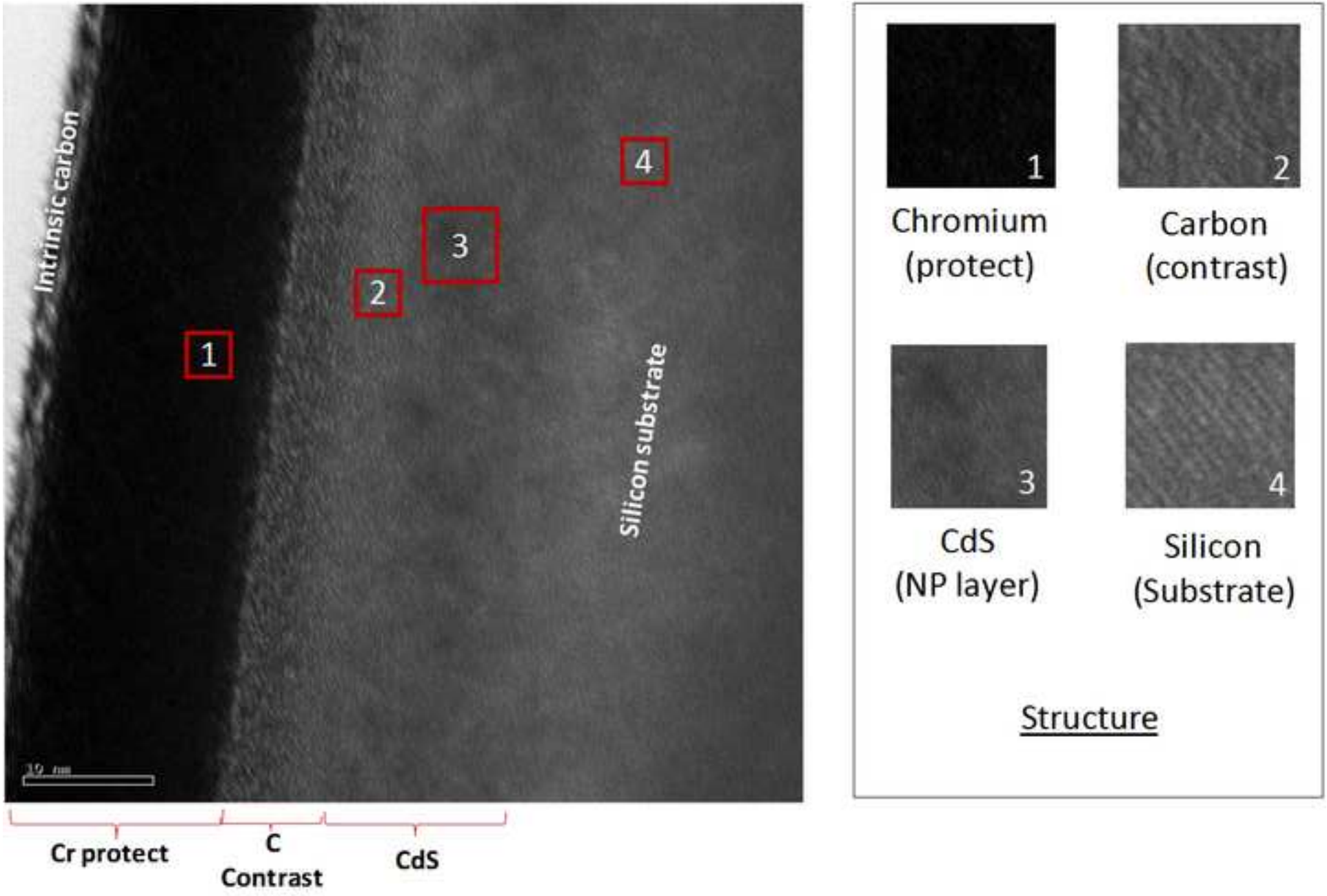

Figure 9

Click here to download high resolution image

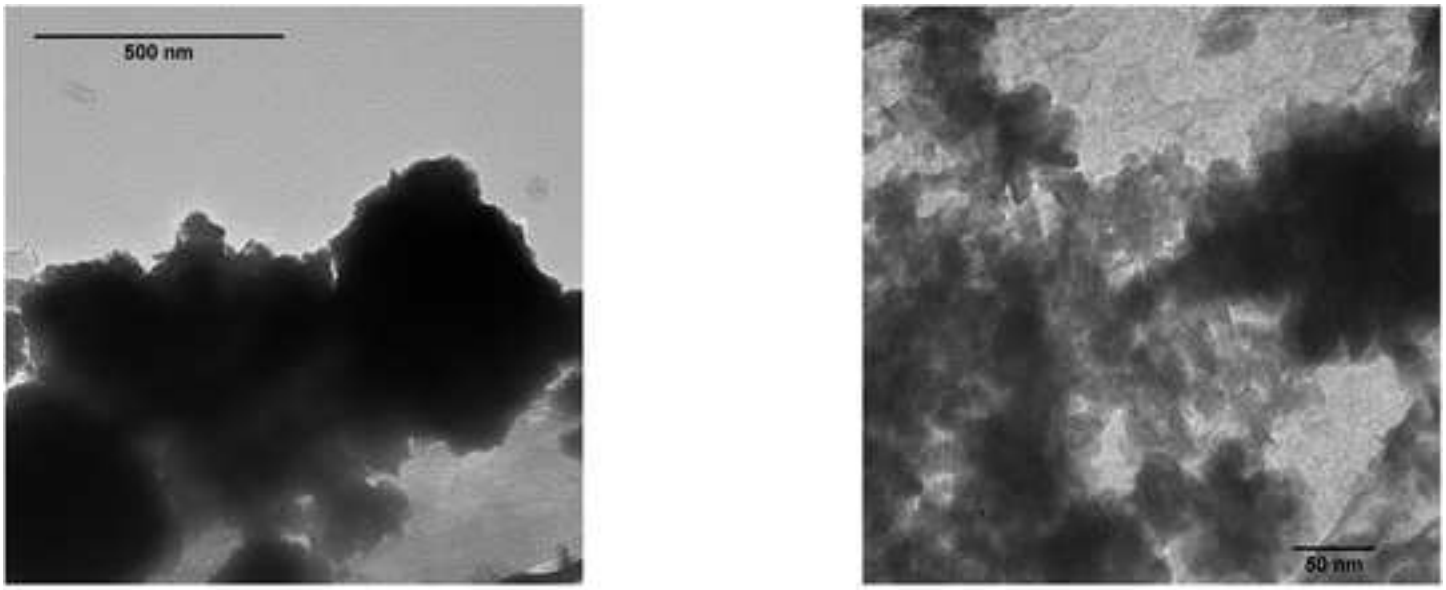

After 1 hr

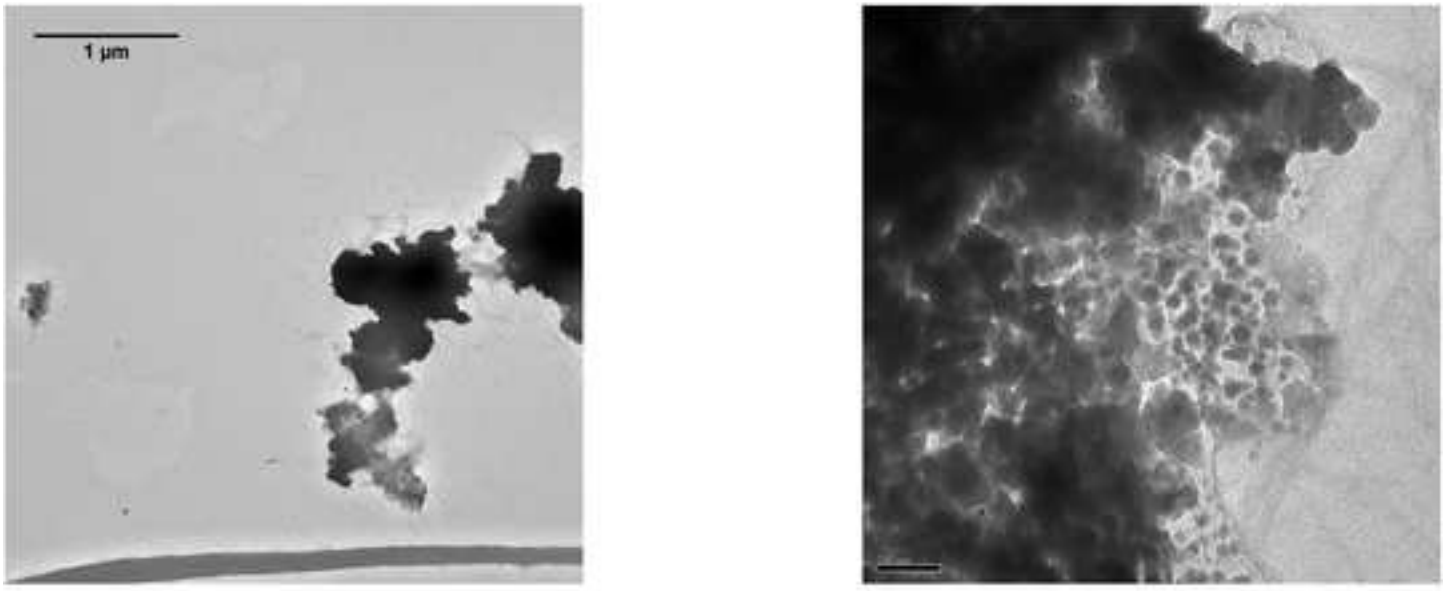

After 2 hr

Figure 10

Click here to download high resolution image

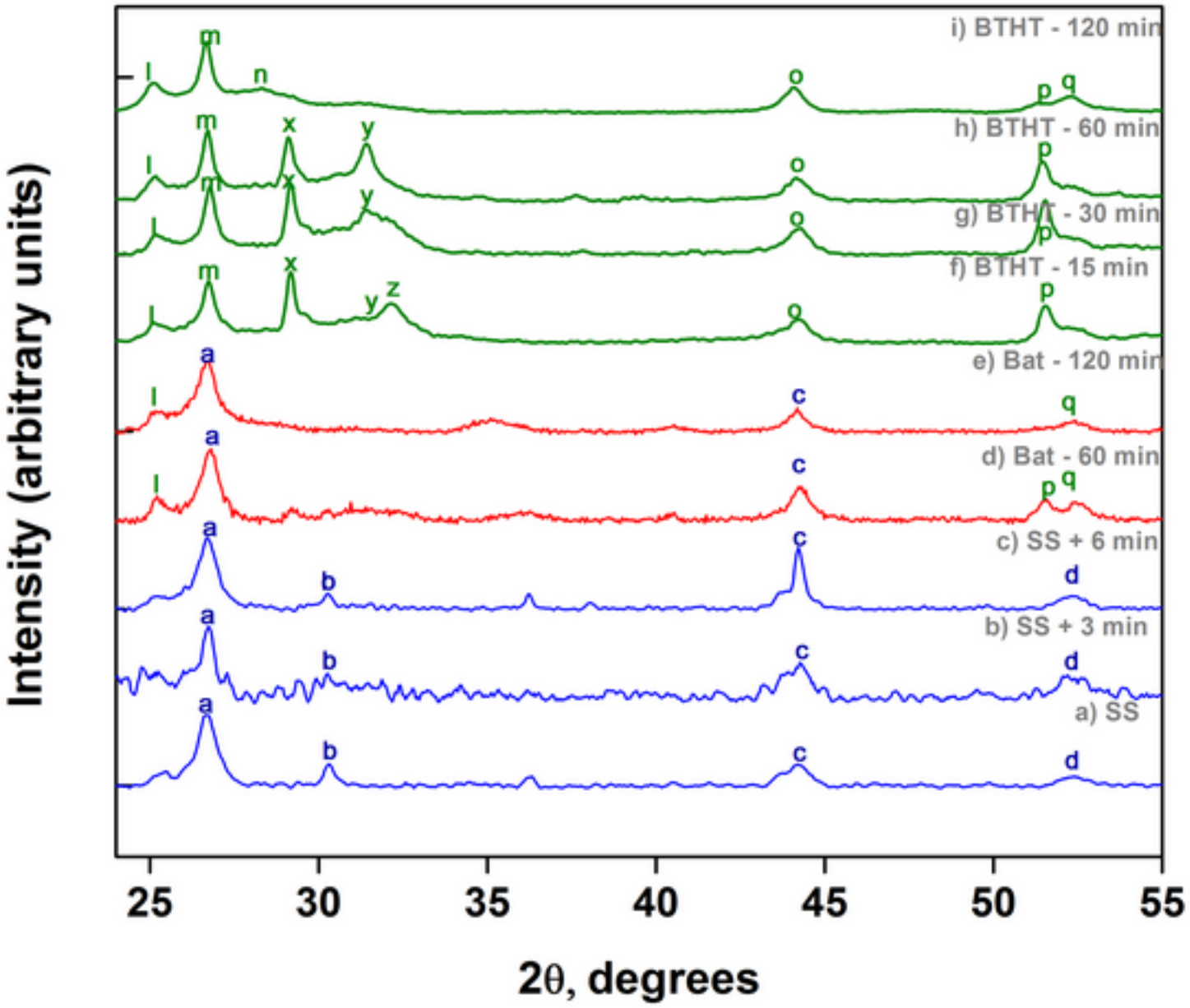

Figure 11

Click here to download high resolution image